Separation Science and Technology
Publication details, including instructions for authors and subscription information:
http://www.informaworld.com/smpp/title~content=t713708471

Adsorption Process Dynamics with Vacuum Purge and Atmospheric Blowdown

Hyeon Lee[a]; Young-Chul Gil[a]; Sung-Sup Suh[b]; Hyung-Keun Song[c]; Sung-Hyun Kim[d]; Dong-Sup Doh[d]
[a] R & D CENTER, DAELIM ENGINEERING CO. LTD., SEOUL, KOREA [b] DEPARTMENT OF CHEMICAL ENGINEERING, HONGIK UNIVERSITY, SEOUL, KOREA [c] DIVISION OF CHEMICAL ENGINEERING, KOREA INSTITUTE OF SCIENCE AND TECHNOLOGY, SEOUL, KOREA [d] DEPARTMENT OF CHEMICAL ENGINEERING, KOREA UNIVERSITY, SEOUL, KOREA

To cite this Article Lee, Hyeon , Gil, Young-Chul , Suh, Sung-Sup , Song, Hyung-Keun , Kim, Sung-Hyun and Doh, Dong-Sup(1996) 'Adsorption Process Dynamics with Vacuum Purge and Atmospheric Blowdown', Separation Science and Technology, 31: 12, 1741 — 1770
To link to this Article: DOI: 10.1080/01496399608000723
URL: http://dx.doi.org/10.1080/01496399608000723

SEPARATION SCIENCE AND TECHNOLOGY, **31**(12), pp. 1741–1770, 1996

Adsorption Process Dynamics with Vacuum Purge and Atmospheric Blowdown

HYEON LEE* and YOUNG-CHUL GIL
R & D CENTER
DAELIM ENGINEERING CO. LTD.
17-5, YOIDO-DONG, YOUNGDUNGPO-KU, SEOUL 150-010, KOREA

SUNG-SUP SUH
DEPARTMENT OF CHEMICAL ENGINEERING
HONGIK UNIVERSITY
SEOUL, KOREA

HYUNG-KEUN SONG
DIVISION OF CHEMICAL ENGINEERING
KOREA INSTITUTE OF SCIENCE AND TECHNOLOGY
SEOUL, KOREA

SUNG-HYUN KIM and DONG-SUP DOH
DEPARTMENT OF CHEMICAL ENGINEERING
KOREA UNIVERSITY
SEOUL, KOREA

ABSTRACT

Experiments with a mathematical model were performed for pure CO_2 feed adsorption on activated carbon up to high pressure (30 kg/cm^2·G) by using H_2 pressurization and vacuum purge to study adsorption steps in vacuum pressure swing adsorption and atmospheric pressure swing adsorption. All on-line real data from transmitters and instruments were obtained using the automatic control and data acquisition system. The maximum breakthrough time and the initial constant pattern were investigated under changing process variables. The maximum breakthrough times were found out under the limiting conditions and compared between two desorption methods using vacuum purge and atmospheric blowdown. The initial constant pattern occurred when the interstitial velocity approached certain

* To whom correspondence should be addressed.

values. The occurrence of the maximum breakthrough curves was strongly related with the formation of the initial constant pattern. From the nonisothermal and nonadiabatic model with the linear driving force model and the temperature-dependent Langmuir isotherms, the effects of the mass and heat transfer parameters on the adsorptive process were examined. The possibility of predicting the breakthrough curves was confirmed by monitoring the temperature propagation profiles. At high pressure the overall heat transfer coefficient had a larger effect on the adsorptive process than the overall mass transfer coefficient.

Key Words. Maximum breakthrough time; Bulk separation; On-line data; Vacuum purge; Mass transfer coefficient; LDF model; Temperature profile

INTRODUCTION

Recently the problems of environmental pollution which has great influence upon human life are on everyone's lips. Air pollution problems are the most serious, so many scientists and engineers look forward to finding clean energy sources instead of using fossil fuels and process systems in order to protect against those problems and simultaneously improve the quality and quantity of products. One system which has been developed is a fixed-bed adsorption system using specified adsorbents. The fixed-bed adsorption system is generally divided into three types of pressure swing adsorption (PSA): vacuum swing adsorption (VSA), temperature swing adsorption (TSA), and combined adsorption (PTSA) (1, 2). The separation systems can also be classified into purification and bulk separation (3) depending on the concentration of the adsorbate. Hydrogen is the most interesting clean energy source because it never produces such environmental pollution materials as CO_2, CO, SO_x, and NO_x. It can be obtained from the outstreams of many industrial processes: methanol reforming gas, coke oven gas (COG), and petrochemical off-gas (2, 4, 5).

Detailed dynamic data of adsorbates and adsorbents are required to design a fixed-bed adsorption system. A number of scientists and engineers have studied single component adsorption modeling for isothermal (6–9) and nonisothermal systems (10–19), and for multicomponent adsorption modeling (20–27). However, most of these papers are confined to dilute systems with a nonadsorbing carrier gas or unreal process systems. A high concentration of strong adsorbate in the feed has seldom been considered.

In our experiment a feed with a pure, strong adsorbate, CO_2, in very high concentration was used for bulk separation. In real bulk component

systems, process conditions such as pressure and feed rate have important effects upon both the concentration and temperature profiles of a fixed bed.

As process conditions change, internal dynamic profiles may become complex or simple according to complicated interactions between the system parameters. Those factors create the limiting conditions for the maximum breakthrough time which is one of the most important operating conditions for the adsorption step in the applications of a practical gas separation process.

The purpose of this paper was to investigate experimentally the maximum breakthrough time for the system of carbon dioxide adsorbed on activated carbon with hydrogen pressurization and vacuum purge or atmospheric blowdown. The effects of pressure and feed rate on the maximum breakthrough time were explored. The present work was therefore undertaken to help find optimum operating variables in vacuum pressure swing adsorption (VPSA) or PSA where the feed has a very high concentration of CO_2 at high pressure.

When constant patterns in concentration were formed, the nonisothermal and nonadiabatic model was used to predict the concentration and temperature profiles in a column. On-line real dynamic data, which rarely exist for the high-pressure range, were obtained and compared with the simulation results.

This project aims to establish the basis for reformer off-gas separation by VPSA or PSA.

MATHEMATICAL MODEL

Prediction of the dynamic behavior inside a column requires simulation results of coupled nonlinear partial differential equations, which include the mass and heat balance equations, to express the internal dynamics. The mass transfer rate between the gas phase and the solid phase was expressed by the linear driving force model (LDF). The adsorption isotherms of CO_2 and H_2 were described by the coupled Langmuir equations. The following approximations were assumed in order to simplify the mathematical model applied to the derivation and calculation.

1. Ideal gas law applies.
2. The axial pressure gradient across the bed is neglected.
3. Plug-flow conditions hold; i.e., axial dispersion is neglected.
4. No variation exists in the radial direction for both concentration and temperature.
5. Temperature-dependent Langmuir isotherms are used.

6. Radial velocity, temperature, and concentration gradients in the bed are neglected.

Mass balances for the gas phase and the solid phase at system pressure P and temperature T are given by

$$\epsilon \frac{\partial uC}{\partial z} + \epsilon \frac{\partial C}{\partial t} + (1 - \epsilon)\rho_p \frac{\partial q}{\partial t} = 0 \tag{a}$$

and

$$\epsilon \frac{\partial uC_i}{\partial z} + \epsilon \frac{\partial C_i}{\partial t} + (1 - \epsilon)\rho_p \frac{\partial q_i}{\partial t} = 0 \tag{b}$$

where C, C_i, q, and q_i are the total concentration, i-component concentration, total adsorbed amount of adsorbate, and the adsorbed amount of i-component adsorbate, respectively. ϵ is the interparticle void fraction. The interstitial velocity, u, is employed.

The energy balance in the column is

$$\left(\epsilon_T + \frac{\rho_B C_{ps}}{\rho_g C_{pg}}\right)\frac{\partial T}{\partial t} + \epsilon \frac{\partial uT}{\partial z} - \frac{\rho_B}{\rho_g C_{pg}} \sum (-\Delta H_i) \frac{\partial q_i}{\partial t} + \frac{4U_o}{\rho_g C_{pg} D}(T - T_0) = 0 \tag{c}$$

where D is the bed diameter.

The LDF model is described by

$$\partial q_i/\partial t = k_i(q_i^* - q_i) \tag{d}$$

The adsorption parameters were experimentally determined by the Langmuir equation as follows (28, 29):

$$q_i^* = \frac{q_{mi} B_i P_i}{1 + \sum_{j=1}^{n} B_j P_j} \tag{e}$$

Equations (a)–(e) and subsidiary equations were transformed into dimensionless equations.

EXPERIMENTAL SYSTEMS AND PROCEDURES

Apparatus and Materials

The experimental apparatus in Fig. 1 was designed for versatile step operations in the VPSA or PSA process under a wide range of process conditions (pressure, temperature, flow rate, etc.) for single- or multicom-

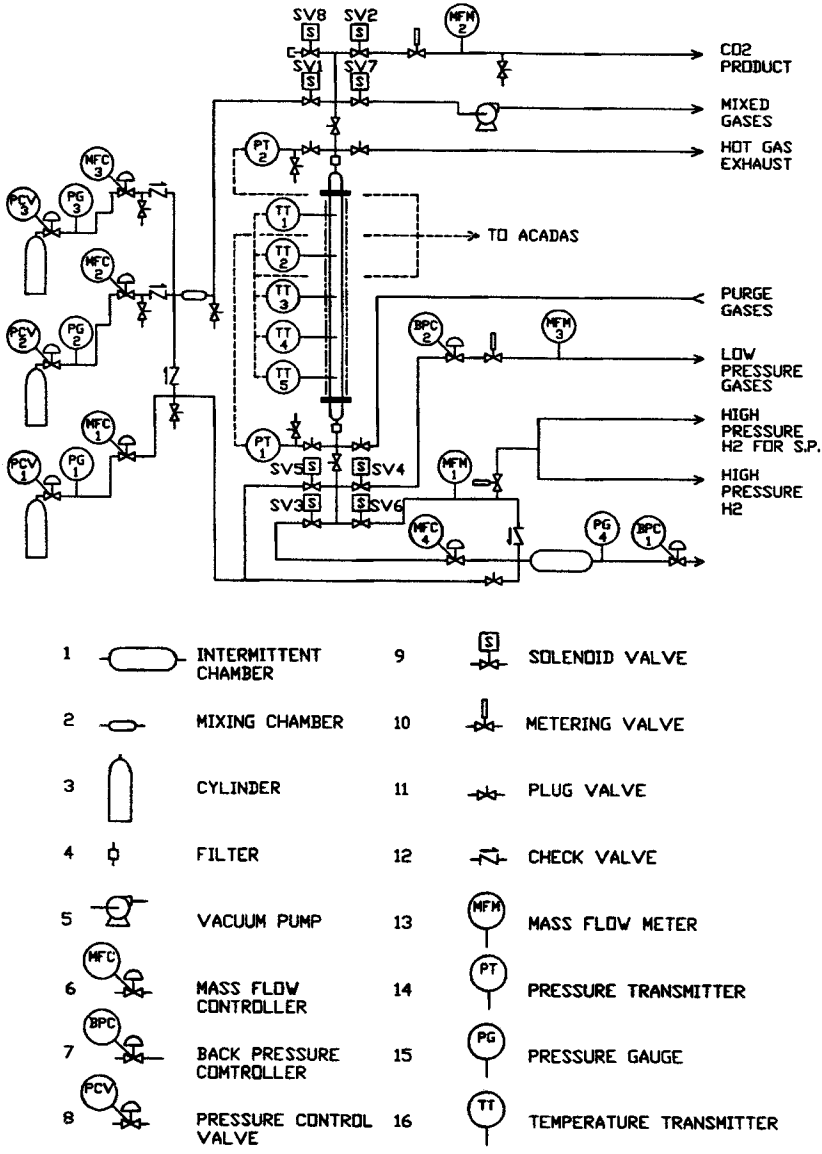

FIG. 1 Schematic drawing of experimental apparatus for VPSA or PSA.

ponent adsorptive separation. All steps were controlled by an automatic control and data acquisition system (ACADAS). All data were on-line monitored and stored in a file. For monitoring and analyzing on-line real concentration data in this system, a residual gas analyzer (RGA, Balzers Co., Model AutoCube 200 Mass Spectrometer) calibrated for system gases was used.

The adsorption column was a 80-cm long and 3.54 cm I.D. stainless steel pipe (type SUS304) filled with 20–30 mesh activated carbon (Samchully Co.). The top suppressor and the bottom supporter of the column were stainless steel perforated double plates where a fine screen for protecting against the loss of large size particles and for distributing the adsorbates was placed. Additional in-line filters (40 μm holes) were installed on both sides of the column to keep fine particles from being entrained into the product and for sampling gas facilities. All lines were 0.25 inch (0.64 cm) stainless steel except for the 0.465 inch (0.95 cm) vacuum line and the 0.0625 inch (0.16 cm) sampling lines.

One pneumatic operated valve (POV) for feed and three electric operated valves (SV) for countercurrent blowdown, vacuum purge, and equalization were installed at the top of the column. Four electrically operated valves which functioned for pressurization, product, cocurrent blowdown, and purge were installed at the bottom of the column. All fluid directions were controlled by setting the valve-opening-time from ACADAS. The feeding system was able to mix gases by mass flow controllers (MFC, Oval Co.) in individual cylinder gas lines. Three check valves were installed in each line upstream of POV for the sake of checking backward flow between feed gases.

An intermittent chamber for the purge step was installed between the product SV and the outlet backpressure controller (BPC, Bronkhorst Co.) which constantly maintained the system pressure. A check valve upstream of the intermittent chamber was placed to maintain high pressure. Purge gas flow was controlled and measured by MFC on that line. The flow rates in cocurrent and countercurrent steps were measured by a mass flow meter (MFM, Oval Co.). An additional BPC was set to fix the cocurrent blowdown pressure. An electric heating system around the column and a refreshing gas line were equipped for adsorbent reactivation and hot purge. In this step the hot fluid made a detour by way of six heatproof block valves (BV) which were adopted to protect the heat-sensitive instruments. Two pressure transmitters (PT, Hartmann & Braun Co.) with pressure ranges up to 40 atm were placed near the inlet and outlet of the column for monitoring and measuring internal pressure.

Temperatures were recorded by five thermocouples (TC, Type K) which were connected to the ACADAS and inserted in the middle of the

packed column at equidistant intervals along the column length. In our ACADAS, all kinds of instruments (PT, TC, MFC, MFM, and BPC) and RGA were linked to microcomputers via interface cards. Also, all valves were operated through ACADAS. It was programmed to monitor and record the data at any interval. For convenience, one second was selected as the time interval in our system.

Procedures

Two kinds of breakthrough experiments were carried out by means of changing degassing steps before the adsorption step. The aim of this breakthrough experiment was to determine the process variables for adsorption steps in the five-step VPSA process and the four-step PSA process. In order to reach the same initial conditions, the following steps were exactly implemented for every run.

In step I, pressurization with H_2 was initiated by opening SV5 connected to MFC1. The column reached the desired pressure by BPC1 connected to the intermittent chamber. In step II, adsorption at high pressure began when SV1 in the top feed line and SV6 downstream of the column opened. Simultaneously, the concentration at the sampling point 1 (SP1) was measured by RGA. The feed rate was controlled by MFC3 for CO_2 while BPC1 kept the system pressure constant. In step III, cocurrent blowdown to the desired pressure was executed by closing both SV1 and SV6 and opening SV4 joined to MFM2. In step IV, countercurrent blowdown to atmospheric pressure was effected by shutting SV4 and opening SV2 connected to MFM3. In step V, vacuum purge was completed by closing SV2 and opening SV7.

For the adsorption step of the four-step PSA process, steps I–IV were the same as those of the above process. In each step of the two processes, all valves were operated at the same time by ACADAS. At the start of the experiments the column was evacuated by a diaphragm vacuum pump for our adsorption step in the five-step VPSA process. The pressure was in the 0.1–30 kg/cm^2 range and the flow rate was in the 3–10 LSTP/min range. The pressurization rate was fixed at 5 LSTP/min.

RESULTS AND DISCUSSION

The experimental breakthrough results were discussed from the following four viewpoints. The first was to determine the flow rate and pressure for the maximum breakthrough time and the relation of breakthrough curves with the formation of a constant pattern. The second was to develop a simple and reasonable simulator for predicting dynamic adsorption

TABLE 1
Operating Conditions

Pressure (kg/cm^2·G)	Flow rate (LSTP/min)
6	3, 5, 7, 9
10	3, 5, 7, 9
15	3, 5, 7, 9, 10
20	3, 5, 7, 9, 10
25	3, 5, 7, 9, 10
30	3, 5, 7, 9, 10

behaviors in the VPSA and PSA processes. The third was to obtain the real dynamic properties at high pressure to be used as reference data for other composition gas systems. The fourth was to confirm the possibility of monitoring the occurrence of breakthrough points using the temperature propagation profiles.

Several experiments were performed at each pressure condition. The operating conditions are given in detail in Table 1. The linear driving force model used to simulate all runs was able to estimate the adsorption characteristics in this experimental system. The characteristics of the adsorption column and some physical properties are given in Tables 2 and 3.

Maximum Breakthrough Time of Adsorption Column

The rising pressure usually makes the adsorption capacity increase and the breakthrough time occur later in the dynamic adsorption. In order to identify the conditions of the maximum breakthrough time and the effect of interstitial velocity on the breakthrough curves, five flow rate conditions were fixed and the pressure was in the 6–30 kg/cm^2·G range.

TABLE 2
Characteristics of Material and Adsorption Bed

Inside diameter, D = 3.541 cm
Bed length, L = 80.0 cm
Interparticle void fraction, ϵ = 0.43
Total void fraction, ϵ_T = 0.778
Average pellet size, a = 0.0718 cm (20–30 mesh)
Particle density, ρ_p = 0.8 g/cm^3
Bed density, ρ_B = 0.4098 g/cm^3

TABLE 3
Adsorbent Heat Capacity (C_{ps}) and Adsorbate Heat Capacity (C_{pg})

Pressure (kg/cm²·G)	Temperature[a] (°C)	Adsorbent heat capacity (cal/g·°C)	Adsorbate heat capacity (cal/g·°C)
6	53.3	0.28413	0.21186
10	53.3	0.28413	0.21190
15	61.7	0.28776	0.21447
20	64.57	0.29263	0.21527
25	70.7	0.30326	0.21705
30	69.5	0.30313	0.21671

[a] Average bed temperatures are used.

The breakthrough curves for the adsorption step following vacuum purge are shown in Figs. 2–6. In the experiments at 3 LSTP/min, as shown in Fig. 2, the breakthrough curves III and IV for 15 and 20 kg/cm²·G, respectively, appear after more time. However, breakthrough curve III becomes more constant than curve IV. In Fig. 3 for 5 LSTP/min, breakthrough curve III for 15 kg/cm²·G occurs earlier than curve IV for 20 kg/cm²·G. The former shows a more constant pattern than the latter. Figure 4 for 7 LSTP/min shows that curve V for 25 kg/cm²·G matches curve IV for 20 kg/cm²·G at the beginning of breakthrough. In Fig. 5 for 9 LSTP/min, curve V of 25 kg/cm²·G does not have an S shape at lower flow rates. The breakthrough time of curve IV for 30 kg/cm²·G approaches that of curve III for 25 kg/cm²·G in Fig. 6 where the flow rate is 10 LSTP/min. It is predicted that a large flow rate will make the curve pattern constant. It is clearly shown in Figs. 2, 3, and 4 that the curves at high pressure fluctuate when the CO_2 concentration is over 50%. These phenomena are caused by the readsorption that occurs near the column outlet.

Up to now it has been shown that the breakthrough time increases with increasing pressure and then decreases above a certain pressure. The maximum breakthrough time decreases with increasing flow rate. Figure 7 shows the effects of flow rate and pressure on the maximum breakthrough time. The earlier occurrence of breakthrough at higher pressure and lower flow rate indicates that the overall mass transfer resistance becomes larger, which results in a decrease of the dynamic adsorption capacity. All the constant pattern curves occurred when the actual interstitial velocity was approximately within a 1.2–1.5 cm/s range.

The breakthrough curves for the high-pressure adsorption step following atmospheric blowdown are shown in Figs. 8–12, where the trends are

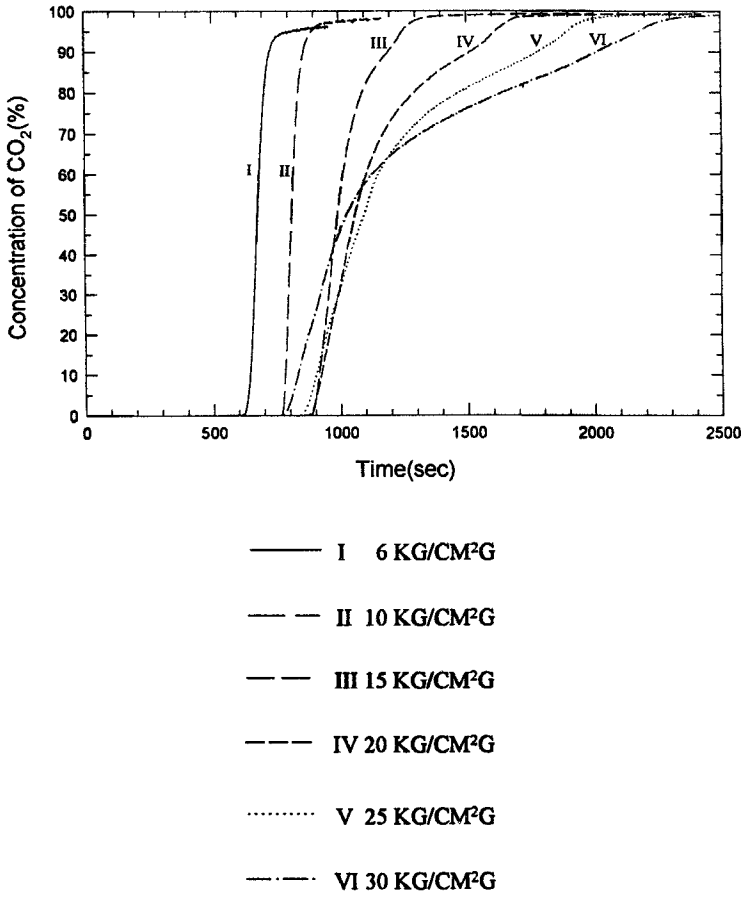

FIG. 2 CO_2 breakthrough curves with various pressures and 3 LSTP-CO_2/min using H_2 pressurization and vacuum purge.

similar to the curves found for vacuum purge. The breakthrough curves after atmospheric blowdown fluctuate less at high pressure than those after vacuum purge. Although the overall tendency for the maximum breakthrough time to occur is quite explicit, the column pressure for the maximum breakthrough time falls within a certain range. This is seen in Fig. 13. The axial dispersion phenomena are dominant in the low CO_2-concentration range. Therefore, it is predicted that axial dispersion prob-

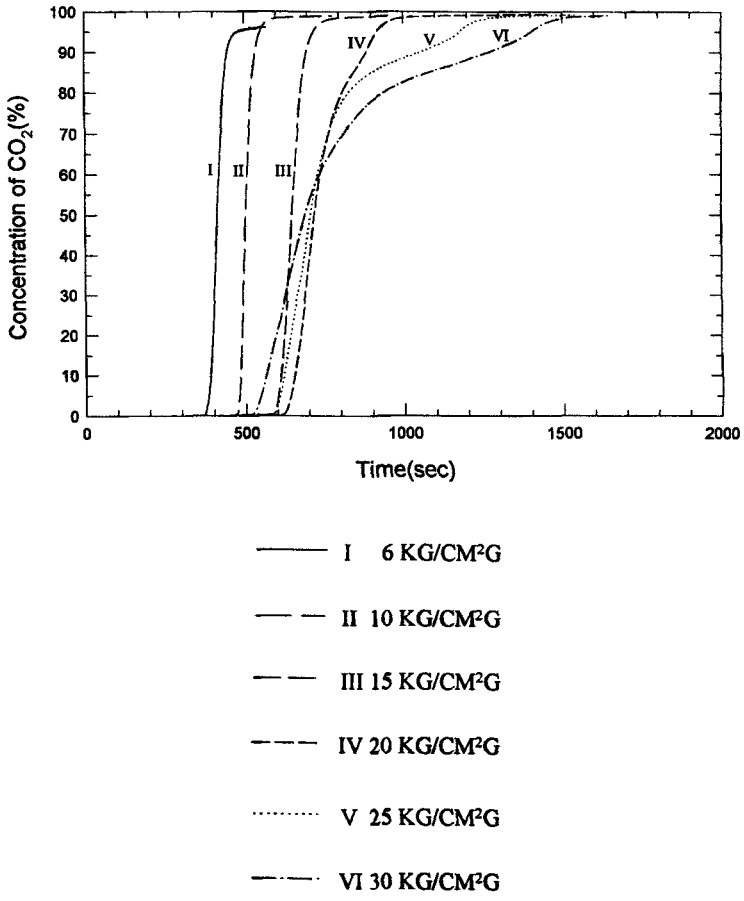

FIG. 3 CO_2 breakthrough curves with various pressures and 5 LSTP-CO_2/min using H_2 pressurization and vacuum purge.

lems will have an unfavorable influence upon the separation processes if a mixture of gases instead of a pure gas is used as the feed.

Comparing Fig. 13 with Fig. 7 shows that the maximum breakthrough time using vacuum purge was the more sensitive to the two process variables. Based on the above fact, decisions about the optimum feed rate and pressure in the VPSA process are more important than those in the PSA process. It was known that an optimum operating pressure exists

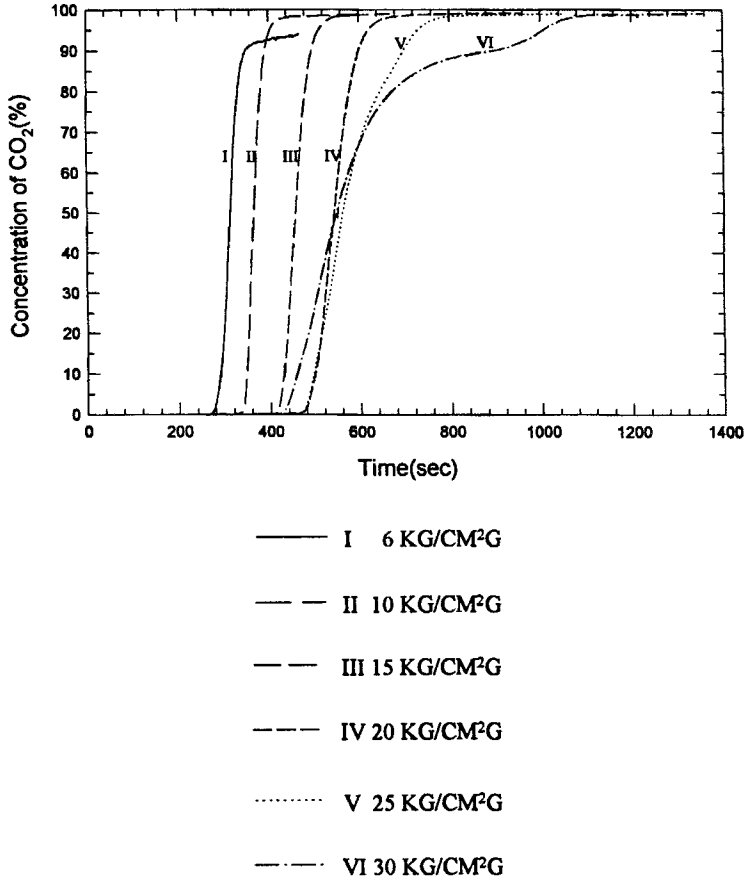

FIG. 4 CO_2 breakthrough curves with various pressures and 7 LSTP-CO_2/min using H_2 pressurization and vacuum purge.

for the equilibrium process (30). Under the mass transfer effect, it is more important to search for the optimum operating pressure.

Comparison of Experimental Data with Numerical Results

In the real VPSA or PSA process, the adsorption step should be terminated before breakthrough occurs. The experimental results showed that

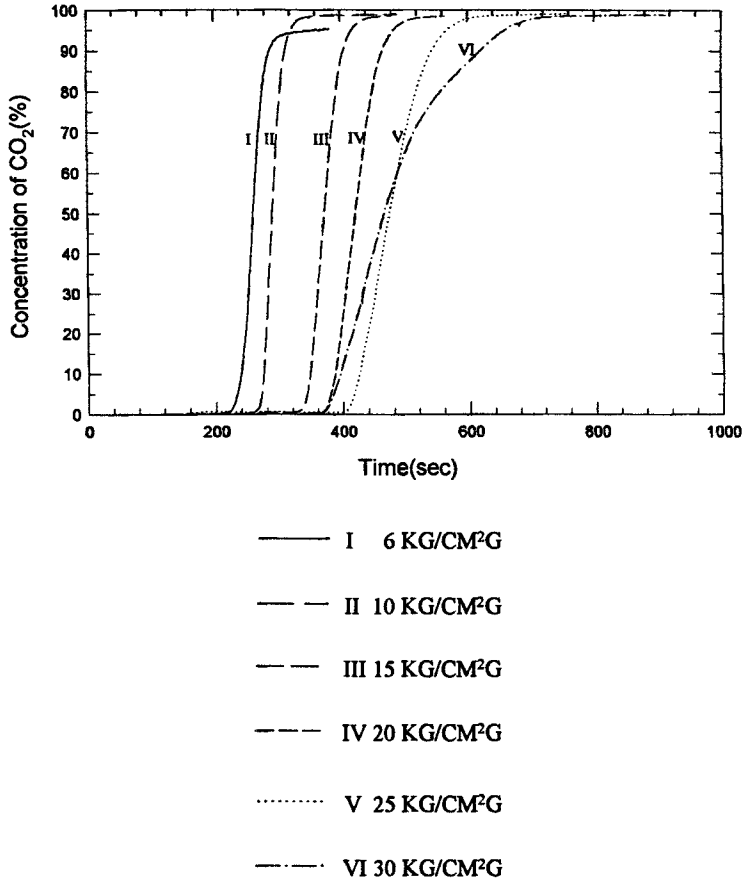

FIG. 5 CO_2 breakthrough curves with various pressures and 9 LSTP-CO_2/min using H_2 pressurization and vacuum purge.

the first constant breakthrough curves in each experimental set had nearly the maximum breakthrough time. Therefore, several runs having maximum breakthrough times were taken into account for developing a good simulator and obtaining practical data which were rarely reported at high pressure. A numerical simulation on the basis of the characteristic properties in Table 2 was performed. The overall mass transfer coefficient, k_{eff}, and the overall heat transfer coefficient, U_o, are obtained as the effective

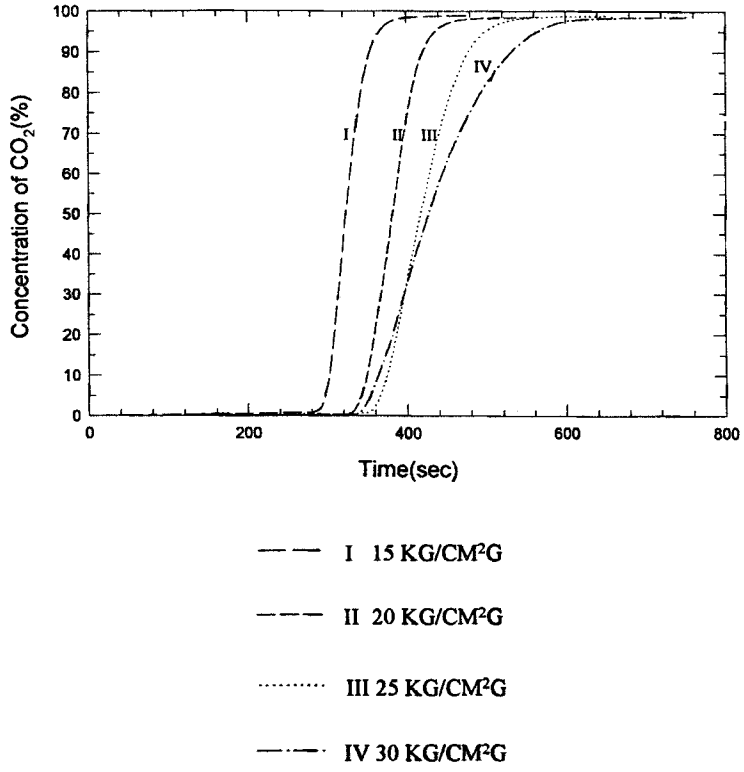

FIG. 6 CO_2 breakthrough curves with various pressures and 10 LSTP-CO_2/min using H_2 pressurization and vacuum purge.

factors for a slim-sized column system. The heat of adsorption for CO_2 on activated carbon (Samchully Co.) was 4100–6400 cal/mol (28, 29). k_{eff} as an adjustable variable was decided upon by fitting the theoretical model to the experimental temperature and concentration profiles. The simulation model satisfactorily described the experimental profiles for all runs using the above parameters.

Relation of Breakthrough Curve with Temperature Profile

Figures 14 through 16 present typical experimental concentration and temperature profiles with the simulation results. The interdistances be-

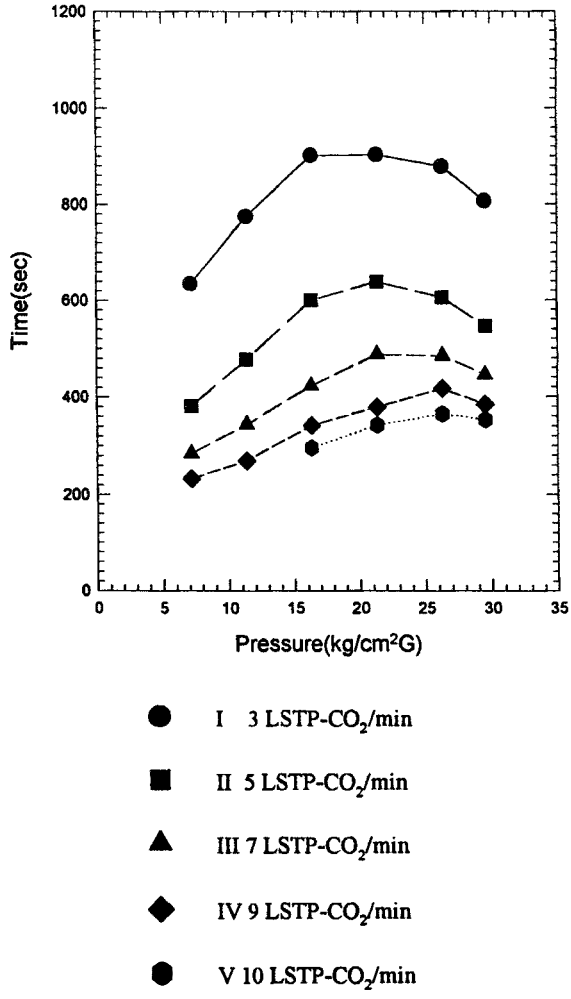

FIG. 7 Breakthrough time with flow rates at 5% of CO_2 concentration using H_2 pressurization and vacuum purge.

tween the take-off points of temperature profiles from the simulation results slightly lengthen with time, which results from the change of the interstitial velocity and neglect of the axial dispersion. This phenomenon was not clearly observed in the experimental results. The simulation temperature profiles increase more sharply at their five take-off points than

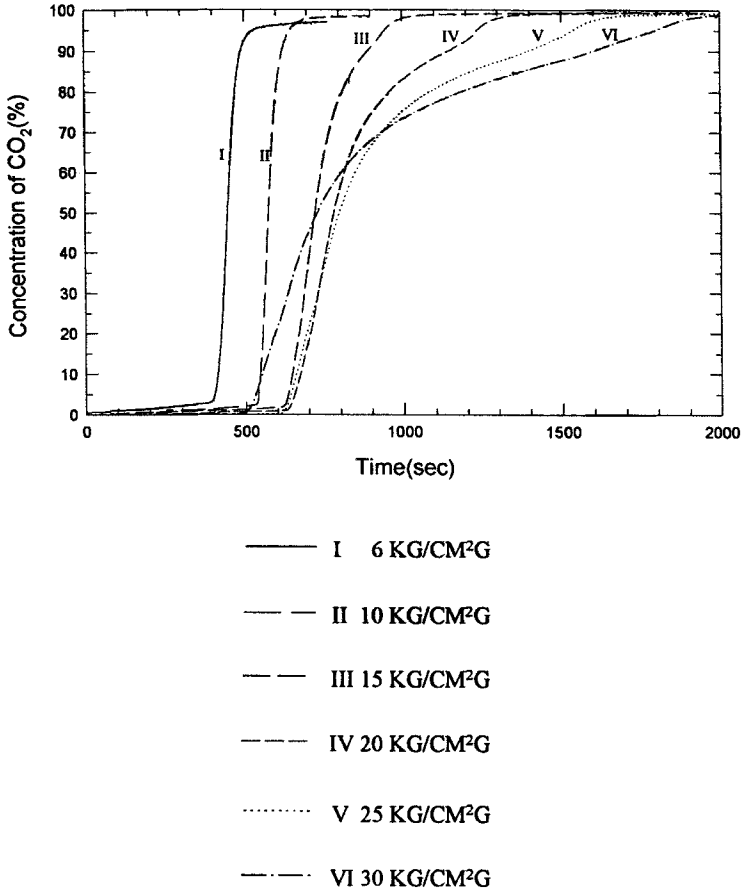

FIG. 8 CO_2 breakthrough curves with various pressures and 3 LSTP-CO_2/min using H_2 pressurization and atmospheric blowdown.

do the experimental temperature profiles. These results mean that the experimental adsorption makes progress slowly and the dynamic adsorption capacity is less than that of the equilibrium state. Also, the simulated concentration curves, which are reasonably accepted in our system, are steeper than those of the experimental data. Those results indicate that dispersion has an effect on our system and dead volume may exist between the column outlet and RGA. Nevertheless, estimating and monitoring the

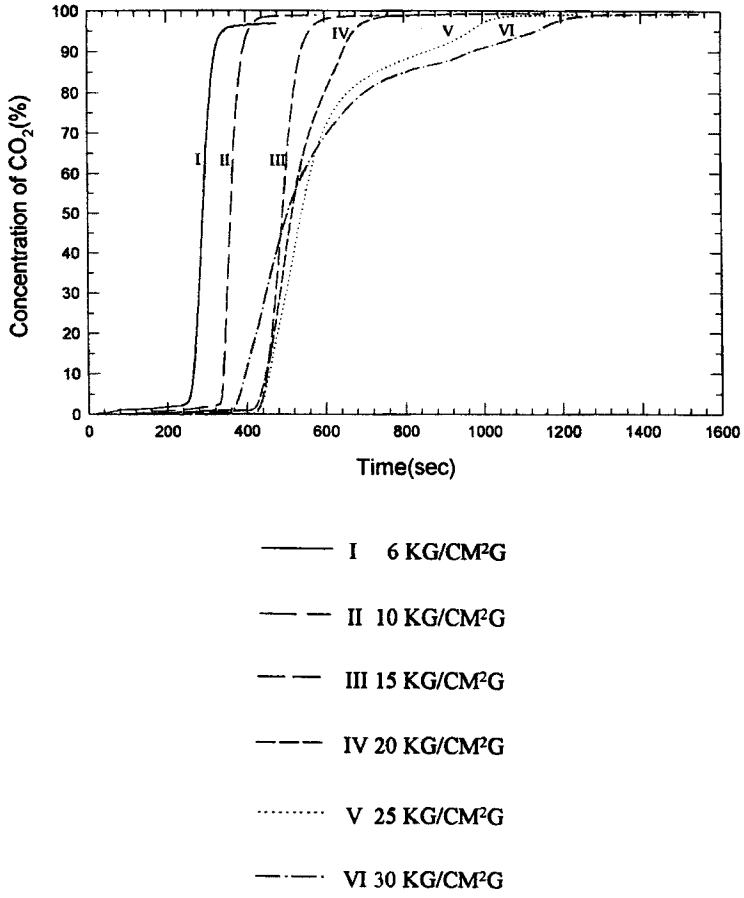

FIG. 9 CO_2 breakthrough curves with various pressures and 5 LSTP-CO_2/min using H_2 pressurization and atmospheric blowdown.

breakthrough time from the temperature propagation profiles does not matter. The temperature in the column rises with increasing pressure with a similar interstitial velocity. In Fig. 14 the temperature differences between the maximum and minimum temperatures along the column length (except for location no. 1) under the same conditions are nearly identical, proving there is the same adsorption capacity at any location without the effect of upstream temperature. Convection flow has an influence upon

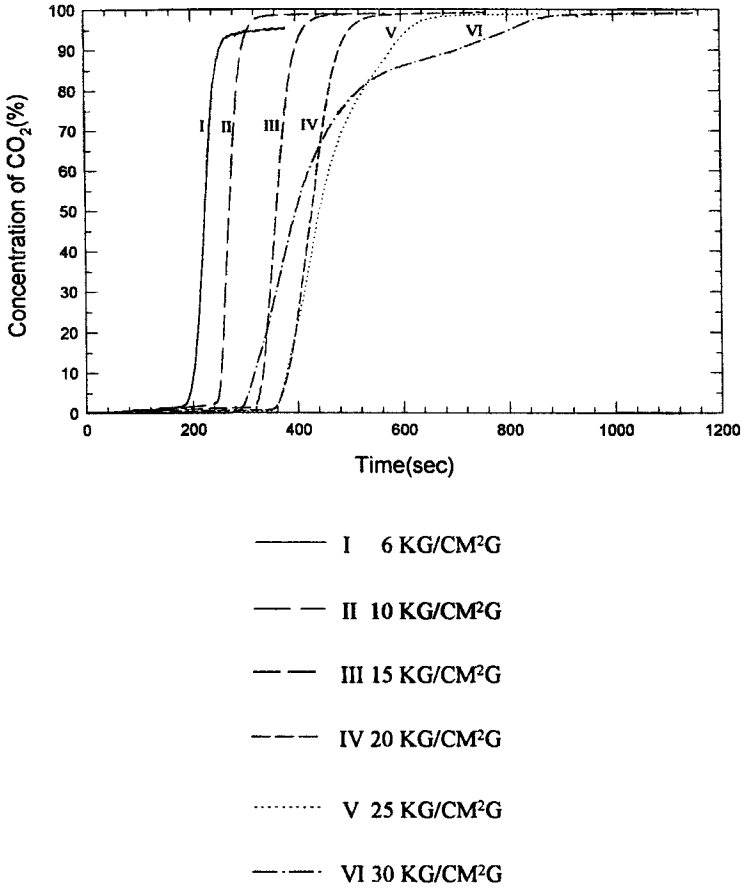

FIG. 10 CO_2 breakthrough curves with various pressures and 7 LSTP-CO_2/min using H_2 pressurization and atmospheric blowdown.

the shape of the temperature profile at location no. 1. The profiles V-a of Fig. 15 and IV-a/V-a of Fig. 16 indicate that the concentration of strong adsorbate is very low in the downstream adsorbent and that the incoming flow leads to the readsorption process, which is why the temperature profiles fluctuate.

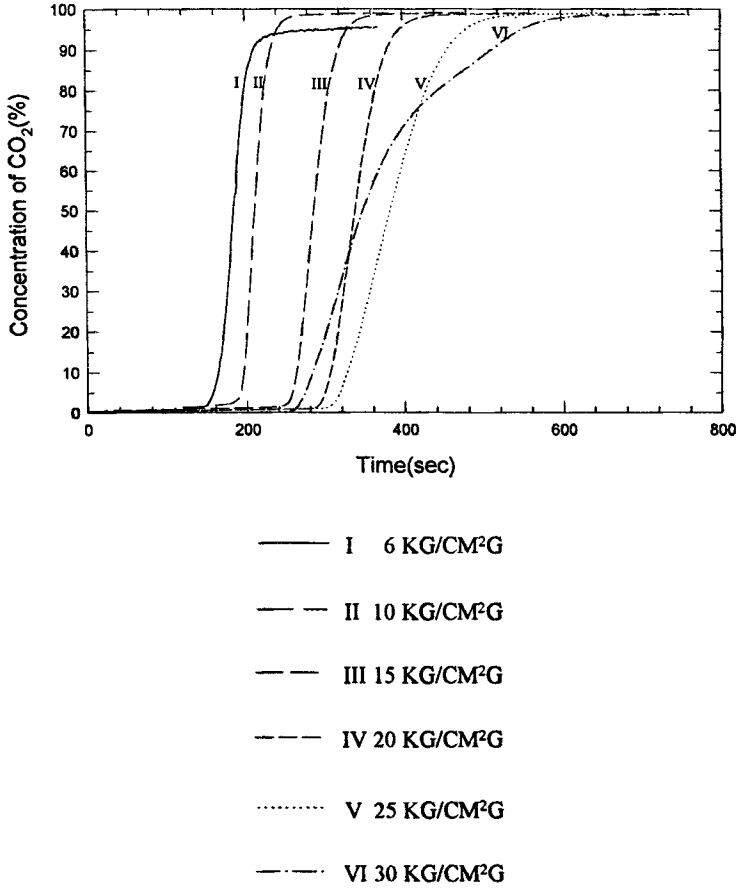

FIG. 11 CO_2 breakthrough curves with various pressures and 9 LSTP-CO_2/min using H_2 pressurization and atmospheric blowdown.

Effects of Pressure on Mass Transfer Coefficient

The overall mass transfer coefficients for the system of carbon dioxide on activated carbon were 0.01–2.0 s^{-1}, depending upon the process conditions. The heat transfer coefficient of 4×10^{-4} cal/(cm^2·s·K) as used here is slightly larger than the data reported in other systems. In Fig. 17 for

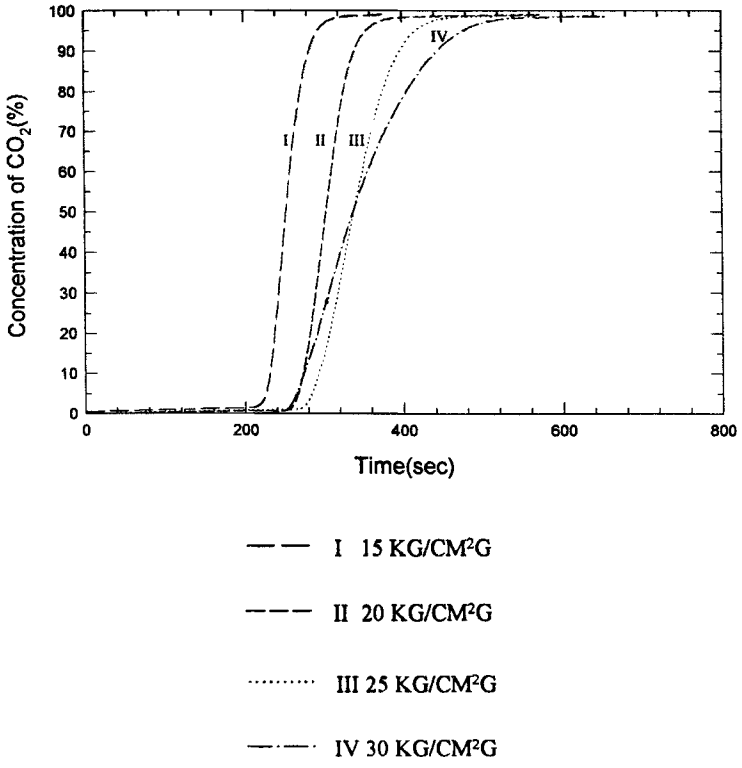

FIG. 12 CO_2 breakthrough curves with various pressures and 10 LSTP-CO_2/min using H_2 pressurization and atmospheric blowdown.

20 kg/cm^2·G and 7 LSTP/min, the mass transfer coefficients within the 0.05–2 s^{-1} range have the breakthrough curve change to a minor degree, i.e., a breakthrough time shift from 486 to 506 seconds. For the bulk adsorptive separation of CO_2 and H_2 on activated carbon, the change of the mass transfer coefficient between 0.05–2 s^{-1} should not have a large influence upon the shape and shift of the breakthrough curve. Similar results were obtained in Fig. 18 for 25 kg/cm^2·G and 9 LSTP/min, and in Fig. 19 for 30 kg/cm^2·G and 10 LSTP/min, by the use of the same mass transfer coefficients.

Raghavan et al. (16) found that the mass transfer coefficient is inversely proportional to pressure if the controlling step in mass transfer is ma-

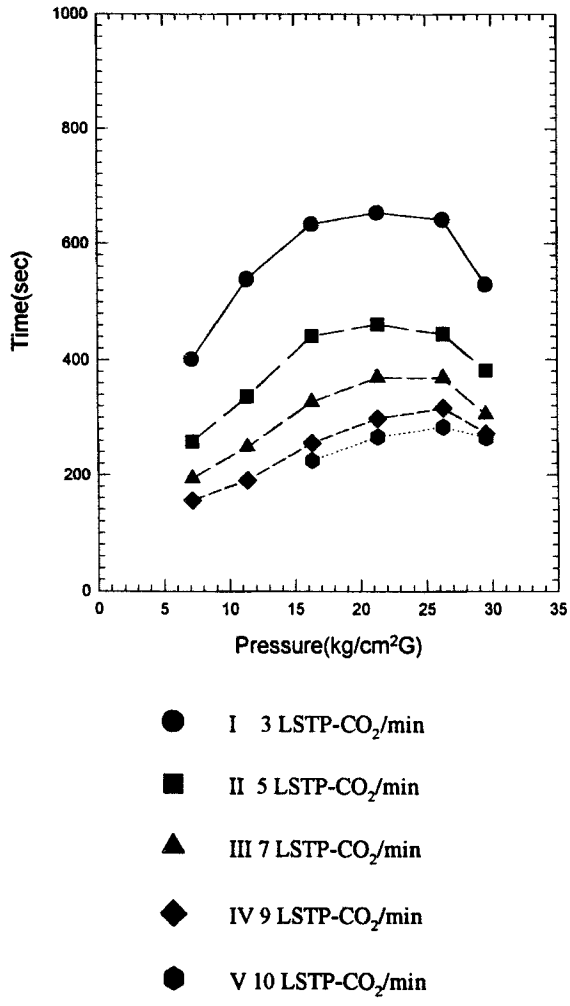

FIG. 13 Breakthrough time with flow rates at 5% of CO_2 concentration using H_2 pressurization and atmospheric blowdown.

cropore diffusion in the molecular regime, while the mass transfer coefficient is effectively independent of pressure within the Knudsen diffusion regime or under conditions of micropore control. In our system, however, the heat transfer coefficient has a large effect on the breakthrough time

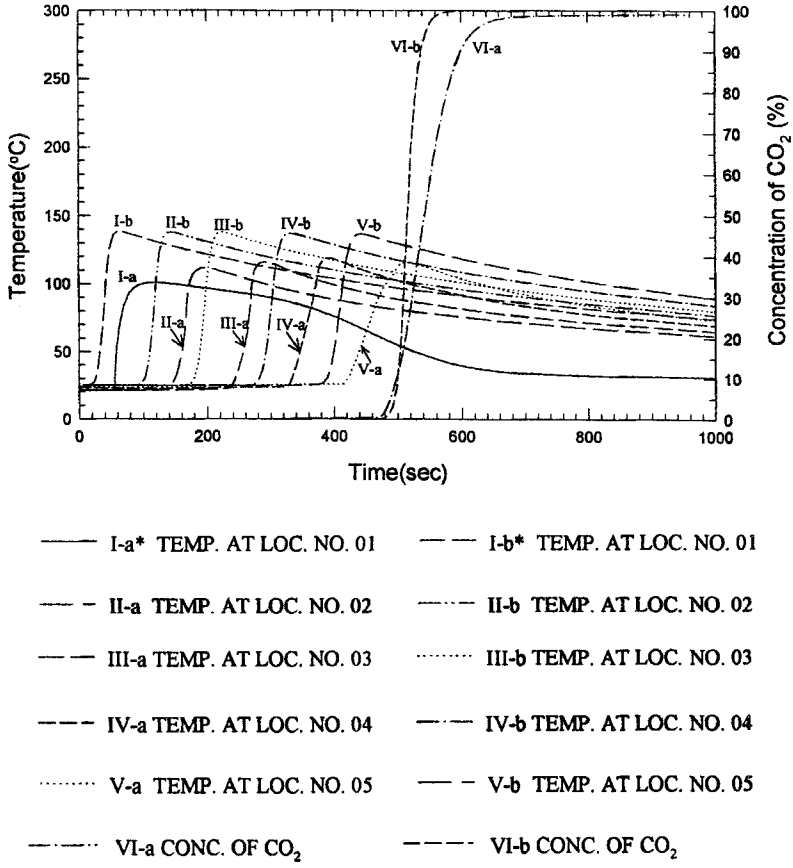

FIG. 14 CO_2 breakthrough curves and temperature profiles at 20 kg/cm^2-G and 7 LSTP-CO_2/min using H_2 pressurization and vacuum purge: (I) loc. no. 01(10 cm), (II) loc. no. 02(25 cm), (III) loc. no. 03(40 cm), (IV) loc. no. 04 (55 cm), (V) loc. no. 05(70 cm) from the top of the column. *Note: Extension a = experimental data, Extension b = simulation data, k_{eff} = 0.1 s^{-1}.

in a slim column system as compared with the effect of the mass transfer coefficient. Although pressure had little effect on the LDF mass transfer coefficient in our simulation results, it was also found that pressure was not an important factor influencing the LDF mass transfer coefficient at high pressure.

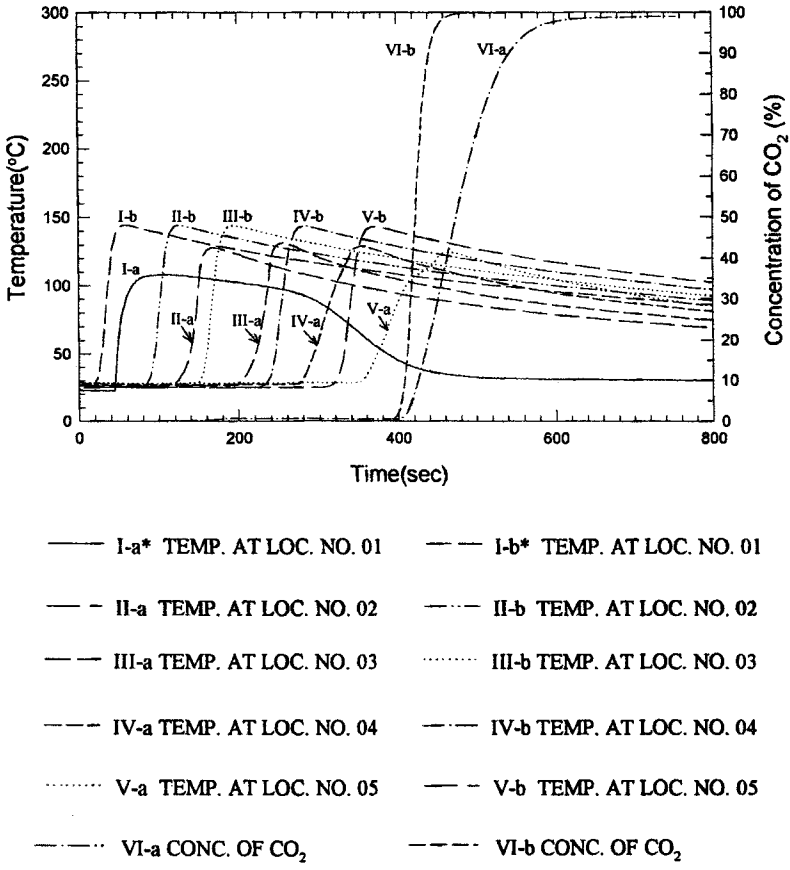

FIG. 15 CO_2 breakthrough curves and temperature profiles at 25 kg/cm^2·G and 9 LSTP-CO_2/min using H_2 pressurization and vacuum purge: (I) loc. no. 01(10 cm), (II) loc. no. 02(25 cm), (III) loc. no. 03(40 cm), (IV) loc. no. 04(55 cm), (V) loc. no. 05(70 cm) from the top of the column. *Note: Extension a = experimental data, Extension b = simulation data, k_{eff} = 0.1 s^{-1}.

Monitoring Solute Movement from Temperature Profiles

A lot of heat was generated by adsorption inside a separation system for bulk separation. Owing to the large quantity of adsorption heat occurring in our system, the most important factor affecting simulation results was the heat transfer rate. When the data of Hwang et al. (19) were used in the present system, the simulation results were not good. In Figs. 14,

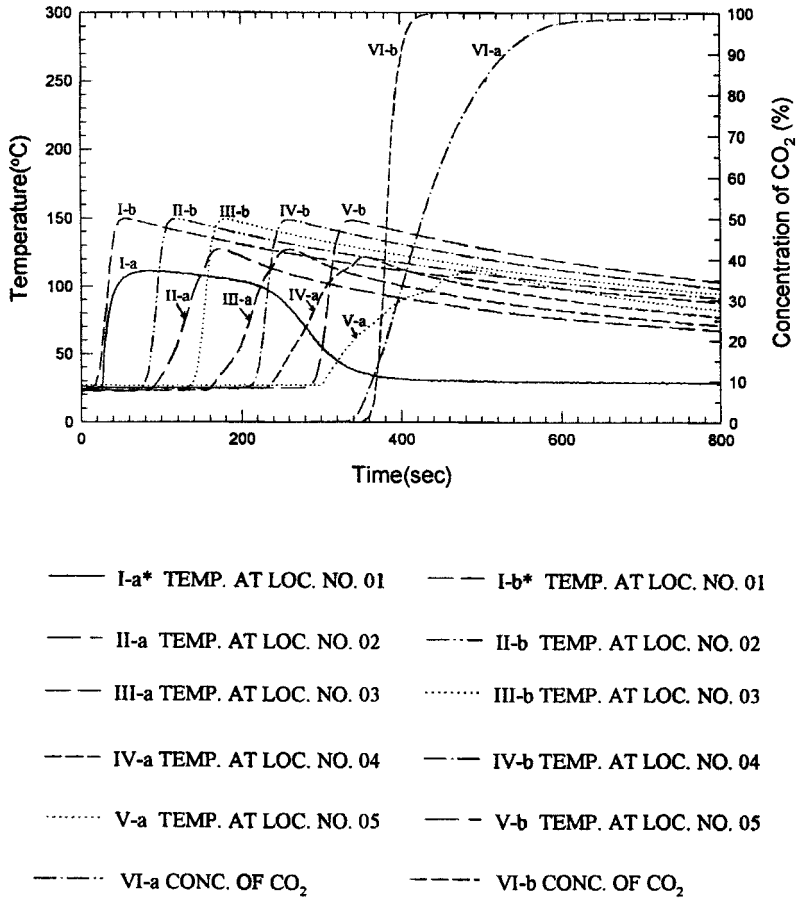

FIG. 16 CO_2 breakthrough curves and temperature profiles at 30 kg/cm^2-G and 10 LSTP-CO_2/min using H_2 pressurization and vacuum purge: (I) loc. no. 01(10 cm), (II) loc. no. 02(25 cm), (III) loc. no. 03(40 cm), (IV) loc. no. 04(55 cm), (V) loc. no. 05(70 cm) from the top of the column. *Note: Extension a = experimental data, Extension b = simulation data, $k_{eff} = 0.1\ s^{-1}$.

15, and 16, the overall heat transfer coefficient (31), $U_o = 4.0 \times 10^{-4}$ cal/(cm^2·s·K), is employed, and the breakthrough curve of simulation results agrees with the experimental breakthrough curve. The take-off time of temperature at each location along the column appears earlier than that of the experimental results.

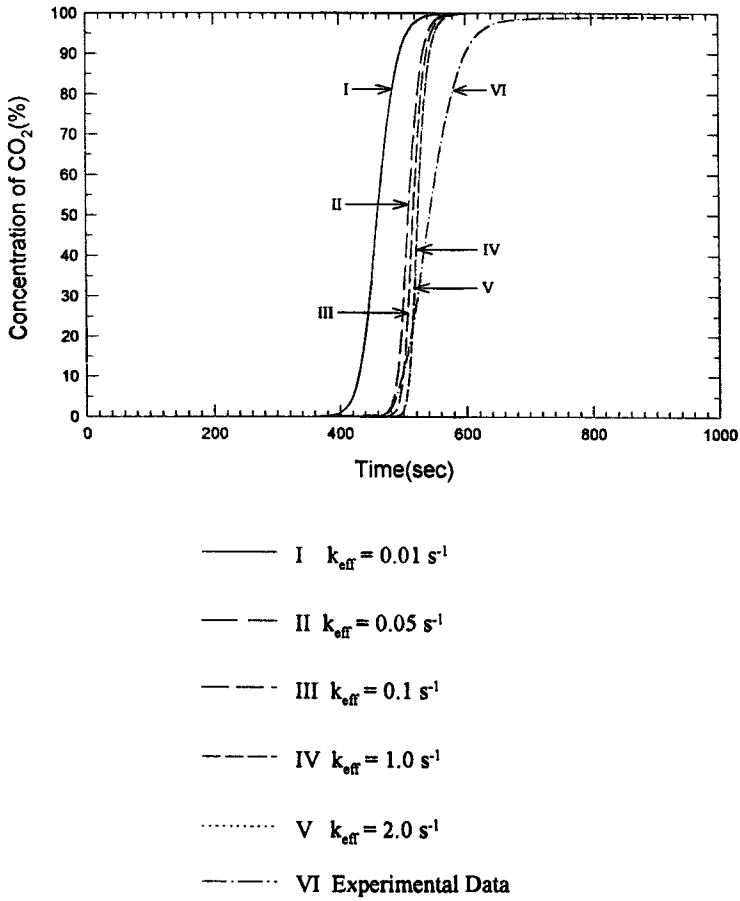

FIG. 17 Effects of k_{eff} on CO_2 breakthrough curves at 20 kg/cm^2-G and 7 LSTP-CO_2/min: (I) k_{eff} = 0.01 s^{-1}, (II) k_{eff} = 0.05 s^{-1}, (III) k_{eff} = 0.1 s^{-1}, (IV) k_{eff} = 1.0 s^{-1}, (V) k_{eff} = 2.0 s^{-1}, and (VI) experimental data.

The shape of the simulation temperature profiles at all locations, except the first location, is similar to that of the experimental temperature profiles. The temperature profile at the first location has a plateau region which is formed by an initial excessive flow rate compared with the downstream flow rate. The phenomena in Fig. 15 are quite similar to those in Fig. 16, exclusive of the plateau shape. It is shown in Figs. 14, 15, and 16 that, as the interstitial velocity increases, the plateau of temperature

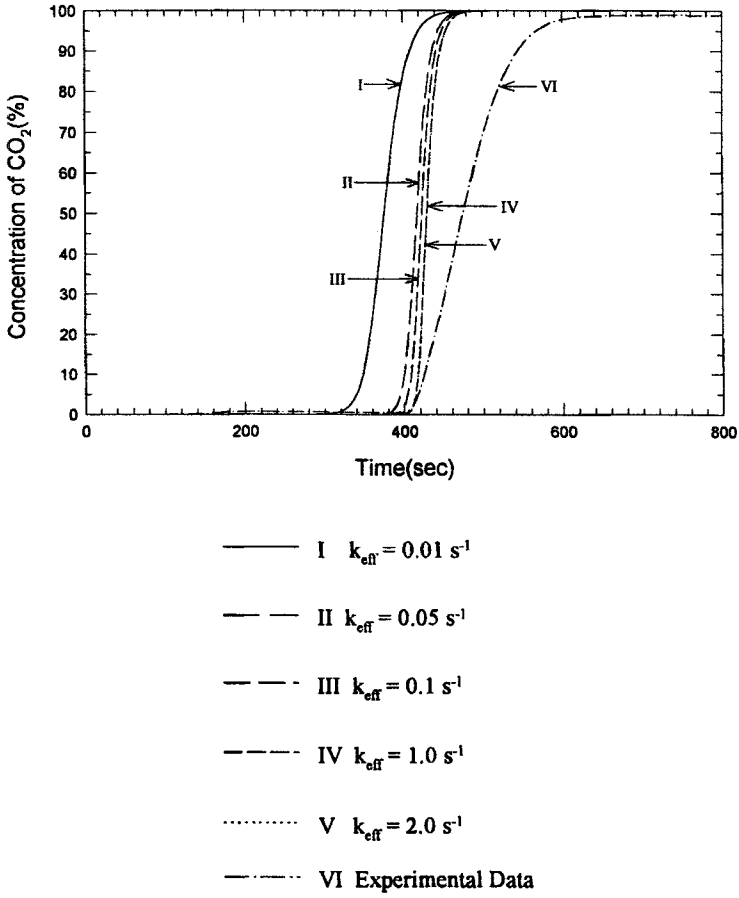

FIG. 18 Effects of k_{eff} on CO_2 breakthrough curves at 25 kg/cm^2-G and 9 LSTP-CO_2/min: (I) k_{eff} = 0.01 s^{-1}, (II) k_{eff} = 0.05 s^{-1}, (III) k_{eff} = 0.1 s^{-1}, (IV) k_{eff} = 1.0 s^{-1}, (V) k_{eff} = 2.0 s^{-1}, and (VI) experimental data.

profile at the first location becomes clear. Similar phenomenon at the next location would appear with increasing flow rate and time. Whether the temperature profiles with a smooth shape have a plateau or not, it is known that the adsorption capacity was fully utilized as a consequence of monitoring the temperature profiles. Although some temperature differences between the experimental and simulation results appear, the propagation rate and trends were approximately similar to each other.

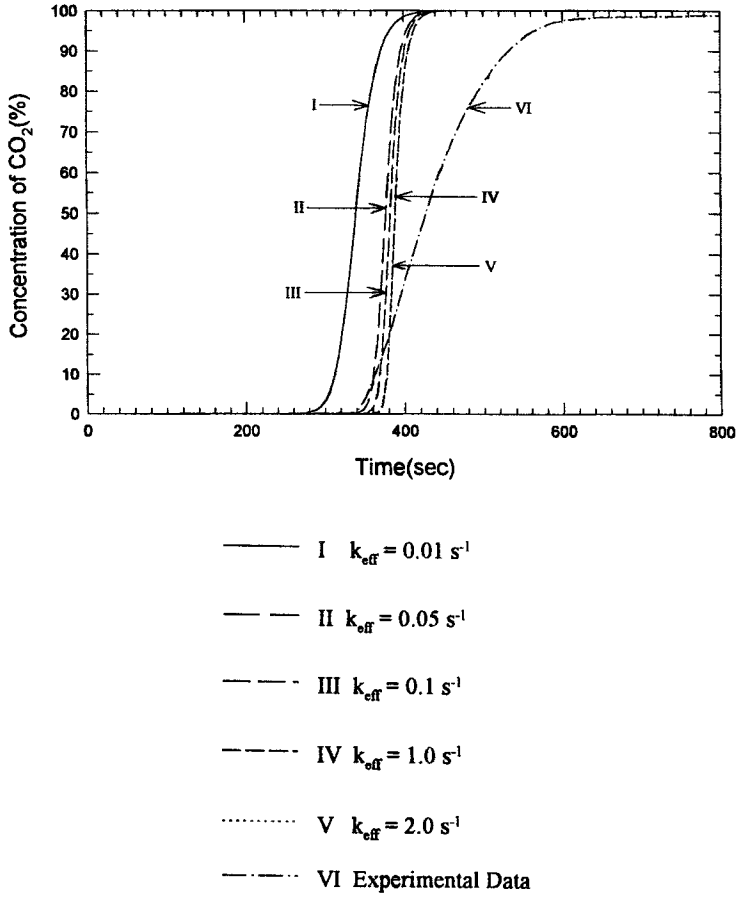

FIG. 19 Effects of k_{eff} on CO_2 breakthrough curves at 30 kg/cm²·G and 10 LSTP-CO_2/min: (I) k_{eff} = 0.01 s^{-1}, (II) k_{eff} = 0.05 s^{-1}, (III) k_{eff} = 0.1 s^{-1}, (IV) k_{eff} = 1.0 s^{-1}, (V) k_{eff} = 2.0 s^{-1}, and (VI) experimental data.

CONCLUSIONS

Two kinds of experiments were performed as a point of reference for the selection of optimum operating variables. One was adsorptive separation under vacuum purge and the other was separation with atmospheric blow-down. From a practical viewpoint, the former is more favorable to the separation process than the latter. In our CO_2 breakthrough experiments,

maximum breakthrough time was found at a certain pressure and flow rate. It occurred at a higher flow rate as the pressure was increased. Also, the maximum breakthrough time using vacuum purge was more sensitive to the two process variables than that using atmospheric blowdown. It was known from the above fact that decisions on optimum feed rate and pressure in the VPSA process were more important than in the PSA process. The breakthrough curves for the maximum breakthrough time were developed with a symmetric pattern in all cases when the interstitial velocity approached the 1.2–1.5 cm/s range.

A simulator suited for modeling a single- or multicomponent adsorptive process on a fixed-bed system was provided to simulate a high-pressure adsorption process dynamically. It was found that pressure was not an important factor influencing the LDF mass transfer coefficient at high pressure. The overall mass transfer coefficient, k_{eff}, within the 0.05–2.0 s^{-1} range had little effect on the concentration and temperature profiles of the model for the present system. However, the heat transfer rate crucially affected the simulation results for the high-pressure and bulk separation system without carrier gas due to the large quantity of heat of adsorption. It was possible to estimate and monitor the breakthrough time from the temperature propagation profiles. Although the temperature of the simulation results deviated somewhat from that of real data, the propagation rate and trends in the experimental and simulation results were generally similar.

As a part of the project of H_2 separation from reformer off-gas, these experiments will be extended to real gas systems. The simulator used here could be developed and applied to VPSA modeling for multicomponent systems.

ACKNOWLEDGMENT

The authors are grateful to Daelim Engineering Co. for their permission to publish this work.

NOMENCLATURE

B_i	Langmuir constant (atm^{-1})
C	concentration of adsorbate in bulk flow (mol/cm^3)
C_i	i-component concentration of adsorbate in bulk flow (mol/cm^3)
C_{pg}	heat capacity of gas (cal/g/K)
C_{ps}	heat capacity of solid (cal/g/K)
D	bed diameter (cm)
K_i	overall mass transfer coefficient (s^{-1})

L	bed length (cm)
P_i	partial pressure (atm)
q	quantity of adsorbate adsorbed (mol/g of solid)
q_i	quantity of i-component adsorbate adsorbed (mol/g of solid)
q_i^*	quantity of i-component adsorbate adsorbed at equilibrium (mol/g of solid)
q_{mi}	quantity of i-component adsorbate adsorbed at monolayer coverage (mol/g of solid)
t	time (s)
T	temperature (K)
T_0	reference temperature (K)
u	interstitial velocity (cm/s)
U_o	overall heat transfer coefficient [cal/(cm^2·K·s)]
z	axial distance along the bed in feed direction (cm)

Greek Letters

ΔH_A	heat of adsorption of adsorbate (cal/mol)
ϵ	interparticle void fraction
ϵ_T	total void fraction
ρ_p	particle density (g/cm^3)
ρ_B	bed density (g/cm^3)
ρ_g	gas density (g/cm^3)

REFERENCES

1. D. M. Ruthven, *Principles of Adsorption & Adsorption Processes*, Wiley, New York, 1984.
2. R. T. Yang, *Gas Separation by Adsorption Processes*, Butterworths, 1987.
3. G. E. Keller, "Industrial Gas Separations," *ACS Symp. Ser.*, *223*, 145 (1983).
4. H. A. Stewart and J. L. Heck, *Chem. Eng. Prog.*, *65*, 78 (1969).
5. C. W. Skarstrom, "Use of Adsorption Phenomenon in Automatic Plant Type Gas Analyzers," *Ann. N. Y. Acad. Sci.*, *72*, 751 (1959).
6. I. Zweibel, *AIChE J.*, *18*, 1139 (1972).
7. D. R. Grag and D. M. Ruthven, *Chem. Eng. Sci.*, *28*, 571 (1973).
8. D. R. Grag and D. M. Ruthven, *Ibid.*, *29*, 1961 (1974).
9. D. R. Grag and D. M. Ruthven, *Ibid.*, *29*, 571 (1974).
10. C. Y. Pan and D. Basmadjian, *Ibid.*, *22*, 285 (1967).
11. C. Y. Pan and D. Basmadjian, *Ibid.*, *25*, 1653 (1970).
12. C. Y. Pan and D. Basmadjian, *Ibid.*, *26*, 45 (1971).
13. S. Fraooq and D. M. Ruthven, *Ind. Eng. Chem. Res.*, *29*, 1076 (1990).
14. S. Fraooq and D. M. Ruthven, *Ibid.*, *29*, 1084 (1990).
15. S. Sircar and R. Kumar, *Ind. Eng. Chem., Process Des. Dev.*, *22*, 271 (1983).
16. N. S. Raghavan and D. M. Ruthven, *Chem. Eng. Sci.*, *39*, 1201 (1984).
17. C. C. Huang and J. R. Fair, *AIChE J.*, *34*, 1861 (1988).
18. C. C. Huang and J. R. Fair, *Ibid.*, *35*, 1667 (1989).

19. K. S. Hwang, J. H. Jun, and W. K. Lee, *Chem. Eng. Sci.*, *50*, 813 (1995).
20. D. O. Cooney and F. P. Strusi, *Ind. Eng. Chem., Fundam.*, *11*, 123 (1972).
21. I. Zwiebel, R. L. Garepy, and J. J. Schnitzer, *AIChE J.*, *20*, 915 (1974).
22. K. Miura, H. Kurahashi, Y. Inokuchi, and K. Harshimoto, *J. Chem. Eng. Jpn.*, *12*, 281 (1979).
23. K. Miura and K. Harshimoto, *Ibid.*, *12*, 329 (1979).
24. J. H. Harwell, A. I. Liapis, R. Lichtfield, and D. T. Hanson, *Chem. Eng. Sci.*, *35*, 2287 (1980).
25. S. Sircar and R. Kumar, *Sep. Sci. Technol.*, *21*, 919 (1986).
26. G. Nagel, G. Kluge, and W. Flock, *Chem. Eng. Sci.*, *42*, 143 (1987).
27. G. Kluge, W. Flock, and G. Nagel, *Ibid.*, *42*, 155 (1987).
28. K. H. Mun, "Adsorption Characteristics of CO, CO_2, H_2 and their Mixtures on Activated Carbon," M.S. Dissertation, Hongik University, Seoul, Korea, 1994.
29. H. B. Lee and S. H. Kim, *J. KIChE*, *1* (1995).
30. S. S. Suh and P. C. Wankat, *Chem. Eng. Sci.*, *44*, 2407 (1989).
31. D. Q. Kern, *Process Heat Transfer*, McGraw-Hill, New York, 1950.

Received by editor September 29, 1995